Nanoscale

ARTICLE

# Size-controlled electron transfer rates determine hydrogen generation efficiency in colloidal Pt-decorated CdS quantum dots

Wei Li,* † Frank Jäckel*

Received 00th January 20xx,
Accepted 00th January 20xx

DOI: 10.1039/x0xx00000x

**www.rsc.org/**

Semiconducting quantum dots (QDs) have been considered as promising building blocks of solar energy harvesting systems because of size-dependent electronic structure, e.g. QD–metal heterostructures for solar-driven $H_2$ production. In order to design improved systems, it is crucial to understand size dependent QD–metal interfacial electron transfer dynamics, picosecond processes in particular. Here, we report that transfer rates of photogenerated electrons in Pt-decorated CdS QDs can be varied over more than two orders of magnitude by controlling the QD size. In small QDs (2.8 nm diameter), conduction band electrons transfer to Pt sites in an average time scale of ~30 ps, giving a transfer rate of $2.9 \times 10^{10}$ $s^{-1}$ while in significantly lager particles (4.8 nm diameter) the transfer rates decrease to $1.4 \times 10^{8}$ $s^{-1}$. We attribute this to the tuning of the electron transfer driving force via quantum confinement-controlled energetic off-set between the involved electronic states of the QD and the co-catalyst, respectively. The same size-dependent trend is observed in presence of an electron acceptor in solution. With methyl viologen presented, electrons leave QDs within less than 1ps from 2.8 nm QDs while for 4.6 nm QDs this process takes nearly 40 ps. The transfer rates are directly correlated with $H_2$ generation efficiencies: faster electron transfer leads to higher $H_2$ generation efficiencies. 2.8 nm QDs display a $H_2$ generation quantum efficiency of 17.3% much higher than that of 11.4% for 4.6 nm diameter counterpart. We explain these difference by the fact that slower electron transfers cannot compete as efficient with recombination and other losses as the faster transfers.

## Introduction

Ensuring a secure and sustainable energy supply is one of the foremost challenges of the 21st century. This challenge mainly stems from the limited supplies of fossil fuels and the need to cut greenhouse gas emissions. Solar radiation, being the largest renewable energy source, will certainly play a major role in any future energy mix. Semiconducting quantum dots (QDs) have been considered as building blocks of solar radiation harvesting systems because QDs can utilize incident photons to generate separated charge carriers in QD sensitized solar cells and photocatalyst systems.[1,2] Efficient transfer of charge carriers across the semiconductor interface is the key for converting solar energy into electricity or fuels.

The most appealing advantage of QDs is their size-dependent electronic structure, which can be applied to design systems with desired electronic and optical properties simply by controlling their size. Particularly, recent work has focused on the importance of QD size in optimizing charge transfer from QDs to various acceptors including oxides, inorganic complexes, organic compounds and carbon allotropes, thus enabling the use of QDs in photovoltaics.[3-7] Charge transfer in each of the aforementioned systems has been recently studied using transient spectroscopic techniques. The dynamics of primary photo-induced processes (i.e. recombination, charge transfer, and trapping) which are crucial to understand the photophysical and photochemical processes in donor–acceptor systems, occur on timescales of sub-picoseconds to nanoseconds and can be studied in great detail using time-resolved photo-luminescence (PL) and ultrafast transient absorption (TA) spectroscopies.[8-11]

QD–metal hybrids that combine the light-harvesting ability of QDs with the catalytic activity of small metal nanoparticles (NPs) show promising applications in photocatalysis, particularly in solar-driven $H_2$ production. In order to design improved systems, it is crucial to understand dynamics and kinetic details of interfacial charge carriers transfer.[12-20] Whereas most of the photocatalytic studies focused on size dependent activity and then connected this with band edge shifts and surface area changes,[21-25] understanding of size dependent QD–metal interfacial electron-transfer dynamics, which is crucial to provide design principle for improved systems, is still lacking.

A number of time-resolved PL measurements have been conducted on CdSe QD-Au NP systems, providing information on the size dependent overall radiative decay processes that extends into the nanoseconds time regime.[26,27] However, early studies have shown that photogenerated charge carriers in a semiconductor nanoparticle can be transferred across the interface in picoseconds.[12-20,28] To probe the size dependent picosecond processes on photocatalytic QD–metal nano-heterostructures for the first time, we employed femtosecond

Department of Physics and Stephenson Institute for Renewable Energy, The University of Liverpool, Chadwick Building, Peach Street, L69 7ZF, Liverpool, UK (fjaeckel@liverpool.ac.uk)
† Present Address: Chemical Engineering & Applied Chemistry, European Bioenergy Research Institute and Aston Institute of Materials Research, Aston University, Aston Triangle, Birmingham B4 7ET, UK (w.li8@aston.ac.uk)
Electronic Supplementary Information (ESI) available: [details of any supplementary information available should be included here]. See DOI: 10.1039/x0xx00000x

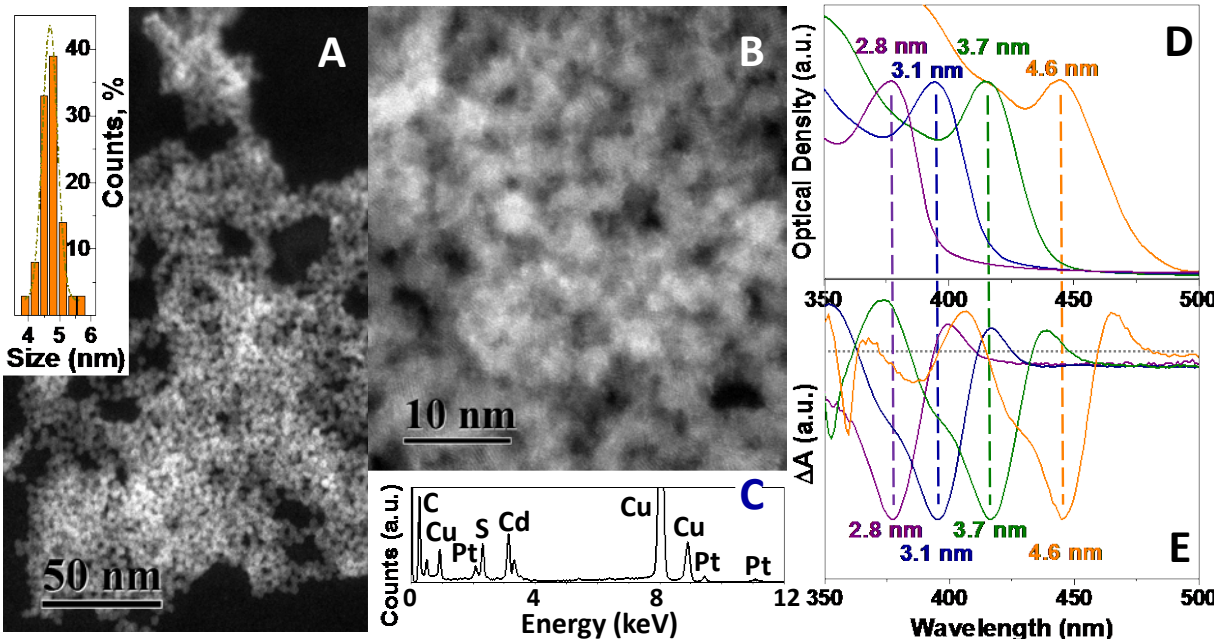


Figure 1 A) STEM image with size distribution (inset) of CdS QDs with an average size of 4.6 nm. B) HAADF-STEM image and C) EDX analysis of Pt/CdS NCs on carbon films coated copper grids. D) Extinction spectra and E) Transient absorption spectra recorded 1 ps following excitation of different size CdS QDs in aqueous solution, horizontal dotted line represents ΔA equal to zero.

transient absorption spectroscopy measurements using 350 nm laser pulses (300 fs). Size-controlled CdS QDs decorated with Pt NPs were synthesized according to reported procedures.[25] An acceleration of the charge carrier dynamics is observed with smaller nanocrystal size which directly correlates with the higher quantum efficiencies for water splitting. A detailed analysis of the transient absorption data establishing this connections with $H_2$ generation efficiencies is reported.

## Results and discussion

Figure 1 illustrates the materials employed. CdS QDs, a widely studied photocatalyst,[13-16,21,22] of different diameters were synthesised in oleic acid/octadecene. The four different controlled diameters are 2.8, 3.1, 3.7 and 4.6 nm as determined from TEM imaging and peak position of the first excitonic transition[29]. They were phase transferred into aqueous solution using cysteine ligands and were decorated with sub-nm Pt clusters according to reported procedures.[15,25] Figure 1A shows a scanning TEM image of the phase transferred CdS NCs. The average size is measured as 4.7 nm with a narrow size distribution (standard deviation of 0.2 nm). Element-sensitive high-angle annular dark field scanning TEM (HAADF-STEM) coupled with energy-dispersive x-ray (EDX) analysis is employed to investigate the morphology of Pt deposited CdS NCs, shown in Figure 1B and 1C. Crystal lattice parameters were measured from Figure 1B and they match with hexagonal wurtzite phase of CdS. The EDX result demonstrates decorated Pt on the NCs was around 13 wt%, which agrees well with the Inductively Coupled Plasma – Optical Emission Spectrometry (ICP-OES) measurement of nearly 16 wt%. HAADF-STEM images of Pt/CdS coupled with EDX analysis confirm that the Pt clusters are well dispersed with a fine size (sub-nm, according to reported value using the same Pt decorating procedures[15]) beyond the detection limit of the instrument. Figure 1D shows the steady-state extinction spectra of the four QDs samples. The narrow and sharp absorption peaks further illustrate the uniform size distribution of all the four sizes NCs. A clear red-shift of the extinction onset and the peak position of the first excitonic transition (1S) is clearly displayed with increasing SNC diameter indicating strong quantum confinement and narrowing of the band gap in the SNCs. It should be noted that Pt/CdS samples show very similar extinction spectra as the corresponding pure QDs samples, i.e. the Pt nanoclusters do not contribute significantly to the overall absorption.

When the CdS QDs suspensions are excited by a 350 nm pump pulse (300 fs), photogenerated electrons and holes will populate the higher energy state and then relax and accumulate to the lower state within the laser pulse duration.[30, 31] Thus, with a delayed probe pulse in the near UV and visible region, a bleach in the absorption can be observed. The recovery of the transient bleach (depletion of absorption) represents the dynamics of the photogenerated electrons and holes at the band edge including charge recombination, trapping and transfer processes. The absorption bleach at the band edge of CdS is dominated by the presence of electrons in the conduction band, while holes at the conduction band edge have negligible contribution.[16, 32, 33] Therefore, the bleaching at the band edge shown in the transient absorption provides an approach to probe the fate of electrons in the conduction band. Figure 1E shows the differential absorption spectra of the different size CdS QDs recorded 1 ps after pump pulse excitation. The bleaching

 

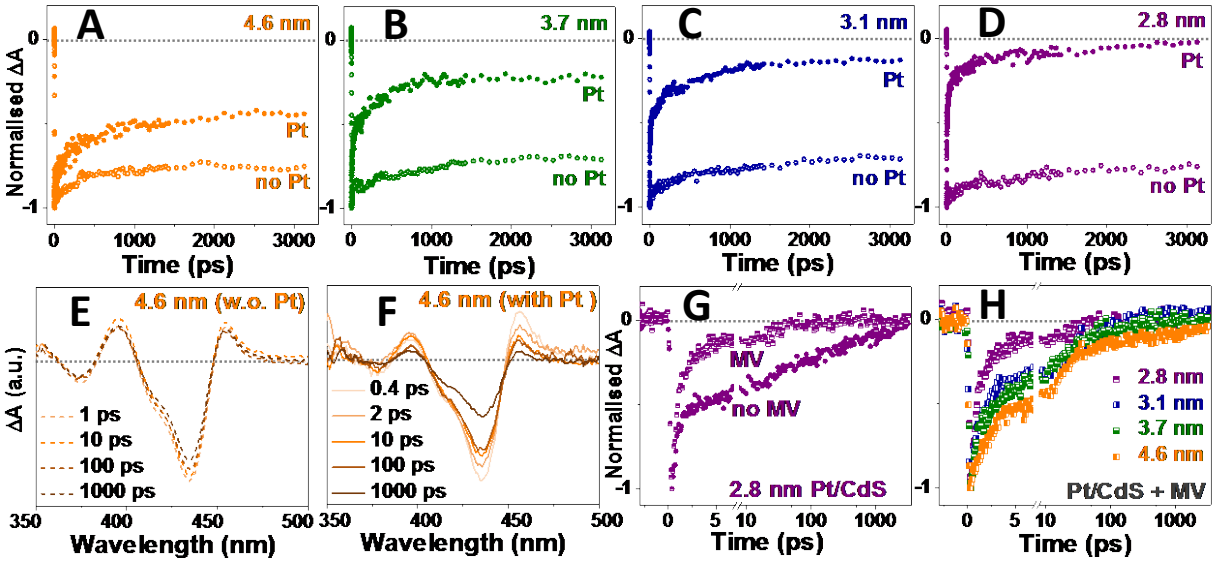


Figure 2: A), B), C) and D) The transient absorption recovery recorded at the bleaching maximum following excitation of four sizes CdS QDs in aqueous solution without and with decorated Pt. Transient absorption spectra of 4.6 nm CdS QDs E) without and F) with decorated Pt at selected time delays. G) The transient bleaching recovery of 2.8 nm Pt/CdS without and with addition of $MV^{2+}$. H) The transient bleaching recovery of four sizes Pt/CdS with addition of $MV^{2+}$.

maximum of each of these different size CdS QDs is consistent with the 1S transition seen in the extinction spectrum.

Figure 2 shows our key results, namely that a clear size dependent of bleaching recovery of Pt/CdS nanocrystals is observed. Before going into the detailed analysis of individual traces, we start with a global discussion of all measurements. In Figure 2A to 2D, there are eight traces of 1S bleach recovery for all the four sizes CdS QDs with and without Pt nanocluster decoration. All measurements show a fast rise at t = 0, followed by three distinct regions (ps fast decay, hundreds of ps decay and a slow ns decay all due to electron relaxation from the 1S state to a new state) in agreement with previous studies.[3-5,17,28,33,34] To quantify these dynamics, the traces were fit with a triple exponential decay convoluted with the instrument response- function (IRF, Table S1). In the absence of Auger recombination (the fluence of the 350 nm pump pulse is selected such that less than 10% of QDs are excited per pulse), initial dynamics are too fast to be associated to either radiative or non-radiative electron and hole recombination back to the ground state. Therefore, the initial fast decays are most possibly due to electron relaxation from the 1S state to a new state in the energy gap (e.g. surface-defect related for CdS, surface-defect related and Pt-CdS interface related for Pt/CdS). It should be noted that, as seen from the spectra in Figure 2E and 2F, the decay of TA signal is spectrally uniform meaning that the multiexponential relaxation behaviour is not related with a size inhomogeneity (which would have resulted a shift of the 1S bleaching).[28]

We now turn to the discussion of the size dependent dynamics. All four CdS QDs sizes without Pt nanocluster decoration show a very similar bleach recovery indicating that the 1S dynamic is not strongly dependent on NC size in the timescale and size range measured here. This is in good agreement with previous reports that the 1S dynamics are mostly affected by NC surface properties rather than NC size.[3-5,28] Since all CdS QDs are prepared in identical procedures, no significant difference in surface properties is expected.

Interestingly, with the presence of Pt nanoclusters, transient bleach recovery of the four sizes QDs becomes remarkably different. First, bleaching of each of these different size Pt/CdS QDs shows faster recovery compared to corresponding QDs samples, because the excited CdS QDs are capable of injecting electrons into the attached Pt nanoclusters; an additional decay channel leads to faster depopulation of the band edge states. In addition and more importantly, a clear acceleration of the dynamics with decreasing nanocrystal size is observed suggesting an increase in transfer rate for the photoelectrons in smaller CdS NCs. Similar phenomena have been observed for charge transfer from QDs to various acceptors including oxides, inorganic complexes, organic compounds and carbon allotropes mainly used for photovoltaics applications.[3-7]

In order to provide more physical insights, we perform a quantitative analysis of our result. If electron transfer to Pt is dominant additional pathway for the excited-state interaction between CdS and Pt, we can evaluate the rate constant by comparing the bleaching recovery lifetimes in the presence and absence of Pt.[17, 34]

$$k_{et} = 1/\tau_{(Pt/CdS)} - 1/\tau_{(CdS)}$$

Table 1: Electron transfer dynamic parameters and quantum efficiency for $H_2$ production

| | Band gap, eV | CdS | | Pt/CdS | | | Pt/CdS + MV | | | IQE, % |
|---|---|---|---|---|---|---|---|---|---|---|
| | | $\tau_{ave}$, ns | $\tau_{1/2}$, ns | $\tau_{ave}$, ps | $\tau_{1/2}$, ps | $k_{et}$, $s^{-1}$ | $\tau_{ave}$, ps | $\tau_{1/2}$, ps | $k_{et}$, $s^{-1}$ | |
| 2.8 nm | 3.15 | 12±1 | > 3* | 34±2 | 3±0.3 | $2.9 \times 10^{10}$ | 0.8±0.3 | 1±0.3 | $1.3 \times 10^{12}$ | 17.3 |
| 3.1 nm | 2.98 | 11±2 | > 3 | 240±10 | 20±4 | $4.1 \times 10^{9}$ | 7±2 | 2±0.3 | $1.4 \times 10^{11}$ | 15.0 |
| 3.7 nm | 2.82 | 10±2 | > 3 | 1100±200 | 100±20 | $8.1 \times 10^{8}$ | 18±2 | 3.5±0.5 | $5.6 \times 10^{10}$ | 13.3 |
| 4.6 nm | 2.58 | 12±1 | > 3 | 4500±700 | 1000±100 | $1.4 \times 10^{8}$ | 37±5 | 7±2 | $2.7 \times 10^{10}$ | 11.4 |

* The slow decay is beyond the temporal range of the delay stage.

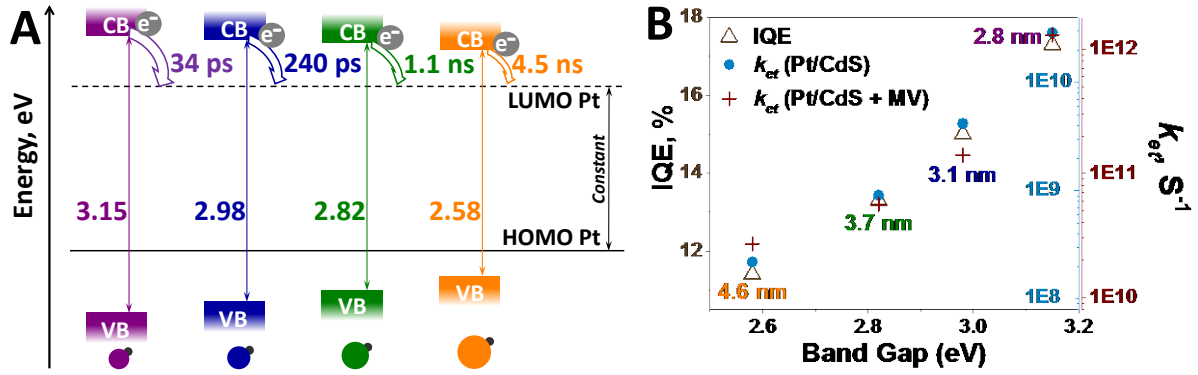


Figure 3: A) Schematic representation of electron transfer rate related to quantum confinement induced energetic off-set between the electronic states of the semiconductor with respect to the co-catalyst. (Adapted from ref. 25. The LUMO position of Pt is only intended as a guide to the eye as we assume a constant HOMO–LUMO-gap for the Pt clusters across the differently sized SNCs.) B) The dependence of $H_2$ efficiency and electron transfer rates on energetic off-sets between QD conduction band edges and the LUMO position of Pt clusters (The band gap data are shown on x-axis since exact values for the off-sets are not available).

For the purpose of this analysis, $\tau$ is calculated as the amplitude-weighted average lifetime ($\tau_{ave} = \sum_i a_i \tau_i$). All calculated results are summarised in Table 1. The fastest electron transfer in the Pt/CdS system was observed with the smallest CdS QDs of 2.8 nm. The rate constant of $2.9 \times 10^{10}$ $s^{-1}$ in this experiment reflects an average lifetime of 34 ps. The rate constants of 3.1, 3.7 and 4.6 nm are $4.1 \times 10^{9}$ $s^{-1}$, $8.1 \times 10^{8}$ $s^{-1}$ and $1.4 \times 10^{8}$ $s^{-1}$ reflecting average lifetimes of 240 ps, 1.1 ns and 4.5 ns, respectively. The electron transfer rate from the smallest CdS QDs to Pt is comparable to typical rates from QDs to various acceptors including oxides, inorganic complexes, organic compounds and carbon allotropes.[3-7] More relevantly, a rate constant of $1.22 \times 10^{9}$ $s^{-1}$ was found from 3.6 nm CdSe QDs to Pt,[17] which is close to that measured here from 3.7 nm CdS QDs to Pt. Half-life times ($\tau_{1/2}$, when 50% of initial signal decays), which is another commonly used parameter in some relevant transient absorption work, follows the same trend and is also included in Table 1.

From the point of view of utilising photogenerated electrons for catalytic reactions, the established size dependent dynamics of electron transfer from CdS to Pt is not sufficient. It is necessary to verify if the size dependent dynamics still holds for an electron involved in an interfacial reaction. Therefore, methyl viologen ($MV^{2+}$, a well-known electron scavenger[35,36]) is employed. The bleach decays more rapidly with the addition of $MV^{2+}$ (see Figure 2G) and it is clear that electron transfer rates are still size dependent (Figure 2H). The kinetic parameters in the presence of MV are summarised in Table 1 as well. In the presence of MV, electrons leave CdS within less than 1ps in 2.8 nm QDs while in 4.6 nm QDs this process needs nearly 40 ps.

The main result of the size dependent electron transfer is illustrated in Figure 3A. Data of band edge positions is adapted from our previous work,[25] demonstrating the widening band gap of smaller QDs in which both conduction and valence band edges shift away from their bulk values due to quantum confinement. The conduction band edge shows an increasing energy offset with smaller NC size relative to the Pt co-catalyst, i.e. larger driving force for electron transfer in the smaller nanocrystals. We thus attribute size dependent electron transfer to tunable electron transfer driving force which is the result of the size-tunable band gap of the nanocrystals. The observed electron transfer rate increases with the driving force, suggesting that the reaction is in the Marcus normal regime.[4, 37] However, a more quantitative analysis applying Marcus Theory as reported elsewhere[5] requires knowledge of the energetic off-sets between the QD conduction band edges and the LUMO position of the Pt clusters, i.e. ΔG. Since the Pt nanoclusters in all Pt/CdS QDs are prepared identically, we expect no significant difference in bulk and defect states (trap, surface, etc.). We therefore conclude that the density of accepting states in Pt has a negligible impact on electron transfer rate in contrast to previous report.[6]

Finally, we correlate the $H_2$ internal quantum efficiency (IQE) of differently sized QDs (data adapted from our previous work[25])

to their electron transfer rates in Figure 3B. In photocatalytic water splitting, 2.8 nm QDs produce $H_2$ in an IQE of 17.3% much higher than that of 11.4% for 4.6 nm diameter counterpart. 3.1 nm and 3.7 nm samples show efficiencies in between and all four data points form a linear trend against band gap. Electron transfer rates of CdS to Pt and Pt/CdS to $MV^{2+}$ are all plotted logarithmically versus band gap and are closely following the trend observed for the IQE.

## Conclusions

In conclusion, ultrafast transient absorption spectroscopy was used to study charge carrier dynamics in size-controlled Pt-decorated CdS QDs. To the best of our knowledge, this is the first time such size dependent picosecond processes of QD−metal nanoheterostructures for photocatalysis is systematically evaluated and correlated with the hydrogen generation efficiencies. Conduction band electrons in 2.8 nm CdS QDs transfer to attached Pt sites in an average time scale of ~30 ps, reflecting a transfer rate of $2.9 \times 10^{10}$ $s^{-1}$, which is more than two orders of magnitude faster than in the 4.6 nm counterpart. We attribute this to a larger driving force for electron transfer in the smaller nanocrystals due to quantum confinement induced increase in the energetic off-set increasing between the electronic states of the semiconductor with respect to the co-catalyst. In the presence of an electron acceptor (e.g. $MV^{2+}$ or $H^+$) in solution, this size dependent charge carrier dynamics still holds, which is utilised for photocatalytic water splitting. An acceleration of charge transfer rates with smaller nanocrystal size is directly correlated with the higher quantum efficiencies for $H_2$ generation. All result provides more quantitative insights and guidance for design of improved systems.

## Experimental details

**Synthesis of Pt-decorated CdS QDs.** The Pt-CdS hybrids were prepared in multiple steps as following: *1) CdS QDs synthesis, following the method of Yu and Peng.*[38] Typically, an 18-g $N_2$ protected mixture of CdO (0.0576 g), oleic acid (0.382 - 3.82 g), and octadecene (90%, technological grade) was heated to 300 °C until the solution became clear and colourless. A solution of sulphur (7.2 mg) dissolved in octadecene (9.0 g) was swiftly injected and the system was cooled down to 250 °C for nanocrystal growth. The size of CdS QDs was controlled by concentration of oleic acid and crystal growth time, and monitored by UV-Vis absorbance[29] (Shimadzu SolidSpec-3700DUV). Monodisperse samples were stored in chloroform. *2) Water transfer of CdS QDs, following the method of Tamang et al.*[39] CdS QDs were then transferred to water by surface treatment with D,L-cysteine hydrochloride resulting in optically clear solutions with an optical density of 1.5 at the first excitonic absorption peak. *3) Pt deposition onto CdS QDs, following previous procedures*.[15, 16, 25] Briefly, 10 mL of OD 1.5 stock solution of CdS QDs (pH 9), 0.15 mL 50 mM chloroplatinic acid hexahydrate, 65 mg ascorbic acid, 650 mg triethanolamine, and 10 mL $H_2O$ were mixed and argon protected in a beaker. UV excitation (ca. 3.5-4 mW/cm$^2$ at 366 nm) from a standard UV lamp was applied for 20 min. Final samples of Pt-CdS hybrids were purified and re-dissolved in distilled water giving a clear yellowish solution with a concentration of OD 0.6.

**Photocatalyst characterization and transient absorption spectroscopy.** The chemical composition of samples was investigated using an Inductively Coupled Plasma – Optical Emission Spectrometry (Spectro Ciros ICP-OES). The morphology of the photocatalyst was characterized with a JEOL JEM-3010 TEM operating at a 300 kV accelerating voltage. Samples for transient absorption measurements exhibited an optical density of 0.5 at their first excitonic absorption peak in a 2 mm cuvette (no visible aggregation observed during measurements in all aqueous solution). Transient absorption measurements employed a commercial laser system (Light Conversion: Pharos ultrafast regenerative amplifier based on Yb:KGW lasing medium, Orpheus optical parametric amplifier, and Lyra second harmonic generation unit) producing 350 nm laser pulses (approximately 200fs, 6 μW excitation above band edges) creating around 0.1 excitons per nanocrystal on average. In this region, recombination is expected to take place by first-order processes.[40] Transient absorption spectra were subsequently acquired with a delayed, low-intensity continuum (360 ~ 480 nm) using a Helios spectrometer (HE-VIS-3200, Ultrafast Systems).

**Photocatalytic reactions and quantum efficiency calculation.** Detailed procedures were set up in previous work.[25] Briefly, hydrogen generation experiments were carried out in a 5 cm long (18.2 mL) cylindrical gastight quartz cuvette with two gas outputs, which is filled with 7 mL solution (containing 3.5 mL Pt/CdS, 0.02 M $Na_2SO_3$ and 0.05 M triethanolamine). Using filtered output of a 450 W Xe lamp, the samples were excited under a beam with 1 cm$^2$ excitation area, 50 mW/cm$^2$ excitation power and spectral range between 350-480 nm. Evolved gas samples were analysed by gas chromatography (Bruker-430-GC) equipped with a thermal conductivity detector. Internal quantum efficiency (IQE) for hydrogen generation (the ratio of photoelectrons consumed for hydrogen production to the number of photons absorbed by the solution) is evaluated with a thermal power sensor (Thorlabs S302C) and a spectrometer (Ocean optics USB4000).

## Conflicts of interest

There are no conflicts to declare.

## Acknowledgements

Financial support by The University of Liverpool (F. J.) is gratefully acknowledged. The authors also acknowledge Dr Alexander Cowan for constructive discussion. The authors further acknowledge support from the EPSRC Laser Loan Pool (EP/G03088X/1). The underlying EPSRC funded data in this paper is available from
http://dx.doi.org/xxx/datacat.liverpool.ac.uk/xxx.

## References


1 A. J. Nozik, M. C. Beard, J. M. Luther, M. Law, R. J. Ellingson and J. C. Johnson, *Chem. Rev.*, 2010, **110**, 6873.
2 M. G. Walter, E. L. Warren, J. R. McKone, S. W. Boettcher, Q. Mi, E. A. Santori and N. S. Lewis, *Chem. Rev.*, 2010, **110**, 6446.
3 A. Kongkanand, K. Tvrdy, K. Takechi, M. Kuno and P. V. Kamat, J*. Am. Chem. Soc.*, 2008, **130**, 4007.
4 J. Huang, D. Stockwell, Z. Huang, D. L. Mohler and T. Lian, *J. Am. Chem. Soc.*, 2008, **130**, 5632.
5 K. Tvrdy, P. A. Frantsuzov and P. V. Kamat, *Proc. Natl. Acad. Sci. U. S. A.*, 2011, **108**, 29.
6 R. B. Liu, B. P. Bloom, D. H. Waldeck, P. Zhang and D. N. Beratan, *J. Phys. Chem. C*, 2017, **121**, 14401.
7 R. B. Liu, B. P. Bloom, D. H. Waldeck, P. Zhang and D. N. Beratan, *J. Phys. Chem. C*, 2018, **122**, 5924.
8 A. O. El-Ballouli, E. Alarousu, M. Bernardi, S. M. Aly, A. P. Lagrow, O. M. Bakr and O. F. Mohammed, *J. Am. Chem. Soc.*, 2014, **136**, 6952.
9 H. J. Yun, T. Paik, B. Diroll, M. E. Edley, J. B. Baxter and C. B. Murray, *ACS Appl. Mater. Interfaces*, 2016, **8**, 14692.
10 Z. H. Xu and M. Cotlet, *Angew. Chem. Int. Ed.*, 2011, **50**, 6079.
11 A. Gocalinska, M. Saba, F. Quochi, M.Marceddu, K. Szendrei, J. Gao, M. A. Loi, M. Yarema, R. Seyrkammer, W. Heiss, A. Mura and G. Bongiovanni, J*. Phys. Chem. Lett.*, 2010, **1**, 1149.
12 P. V. Kamat, *J. Phys. Chem. Lett.*, 2012, **3**, 663.
13 K. F. Wu, H. M. Zhu, Z. Liu, W. Rodríguez-Córdoba and T. Q. Lian, *J. Am. Chem. Soc.*, 2012, **134**, 10337.
14 K. F. Wu, Z. Y. Chen, H. J. Lv, H. M. Zhu, C. L. Hill and T. Q. Lian, *J. Am. Chem. Soc.*, 2014, **136**, 7708.
15 M. J. Berr, A. Vaneski, C. Mauser, S. Fischbach, A. S. Susha, A. L. Rogach, F. Jäckel and J. Feldmann, *Small*, 2012, **8**, 291.
16 W. Li, J. R. Lee and F. Jäckel, *ACS Appl. Mater. Interfaces*, 2016, **8**, 29434.
17 C. Harris and P. V. Kamat, *ACS Nano*, 2010, **4**, 7321.
18 C. Gimbert-Suriñach, J. Albero, T. Stoll, J. Fortage, M. N. Collomb, A. Deronzier, E. Palomares and A. Llobet, *J. Am. Chem. Soc.*, 2014, **136**, 7655.
19 J. R. Lee, W. Li, A. J. Cowan and F. Jäckel, *J. Phys. Chem. C*, 2017, **121**, 15160.
20 Y. Ye, X. L. Wang, S. Ye, Y. X. Xu, Z. C. Feng and C. Li, *J. Phys. Chem. C*, 2017, **121**, 17112.
21 S. Yanagida, T. Ogata, A. Shindo, H. Hosokawa, H. Mori, T. Sakata and Y. Wada, *Bull. Chem. Soc. Jpn.*, 1995, **68**, 752.
22 K. Ogisu, K. Takanabe, D. L. Lu, M. Saruyama, T. Ikeda, M. Kanehara, T. Teranishi and K. Domen, *Bull. Chem. Soc. Jpn.*, 2009, **82**, 528.
23 J. Zhao, M. A. Holmes and F. E. Osterloh, *ACS Nano*, 2013, **7**, 4316.
24 S. K. Apte, S. N. Garaje, S. D. Naik, R. P. Waichal, J. O. Baeg and B. B. Kale, *Nanoscale*, 2014, **6**, 908.
25 W. Li, G. O'Dowd, T. J. Whittles, D. Hesp, Y. Gründer, V. R. Dhanak and F. Jäckel. *Nanoscale*, 2015, **7**, 16606.
26 M. Kondon, J. Kim, N. Udawatte and D. Lee, *J. Phys. Chem. C*, 2008, **112**, 6695.
27 U. Soni, P. Tripathy and S. Sapra, *J. Phys. Chem. Lett.*, 2014, **5**, 1909.
28 V. I. Klimov, D. W. McBranch, C. A. Leatherdale and M. G. Bawendi, *Phys. Rev. B*, 1999, **60**, 13740.
29 W. W. Yu, L. H. Qu, W. Z. Guo, and X. G. Peng, *Chem. Mater.*, 2003, **15**, 2854.
30 D. J. Norris and M. G. Bawendi, *Phys. Rev. B*, 1996, **53**, 16338.
31 V. I. Klimov and D. W. McBranch, *Phys. Rev. Lett.*, 1998, **80**, 4028.
32 S. Logunov, T. Green, S. Marguet and M. A. El-Sayed, *J. Phys. Chem. A,* 1998, **102**, 5652.
33 J. Z. Zhang, *J. Phys. Chem. B*, 2000, **104**, 7239.
34 I. Robel, M. Kuno and P. V. Kamat, *J. Am. Chem. Soc.*, 2007, **129**, 4136.
35 T. Simon, M. T. Carlson, J. K. Stolarczyk and J. Feldmann, *ACS Energy Lett.*, 2016, **1**, 1137.
36 J. L. Ellis, D. D. Hickstein, K. J. Schnitzenbaumer, M. B. Wilker, B. B. Palm, J. L. Jimenez, G. Dukovic, H. C. Kapteyn, M. M. Murnane and W. Xiong, *J. Am. Chem. Soc*., 2015, **137**, 3759.
37 P. A. Marcus and N.Sutin, *Biochem. Biophys. Acta*, 1985, **811**, 265
38 W. W. Yu and X. G. Peng, *Angew. Chem. Int. Ed.*, 2002, **41**, 2368.
39 S. Tamang, G. Beaune, I. Texier and P. Reiss, *ACS Nano*, 2011, **5**, 9392.
40 N. Serpone, D. Lawless and R. Khairutdinov, *J. Phys. Chem.*, 1995, **99**, 16655.


 